

# Bulletin of the Seismological Society of America

Vol. 79

December 1989

No. 6

## SITE AMPLIFICATION AND ATTENUATION OF STRONG GROUND MOTION

BY SANDRA H. SEALE AND RALPH J. ARCHULETA

### ABSTRACT

At the McGee Creek, California, site, three-component strong-motion accelerometers are located at depths of 166 m, 35 m, and 0 m. The surface material is glacial moraine, to a depth of 30.5 m, overlying hornfels. Accelerations were recorded from two California earthquakes: Round Valley,  $M_L$  5.8, 23 November 1984, 18:08 UTC and Chalfant Valley,  $M_L$  6.4, 21 July 1986, 14:42 UTC. Anti-plane shear strains for the Round Valley and Chalfant Valley events are less than  $1.8 \times 10^{-5}$  and  $1.2 \times 10^{-5}$ , respectively. By separating out the *SH* components of acceleration, we were able to determine the orientations of the downhole instruments. Peak *SH* accelerations at the surface were 5.7 times greater than those at 166 m in both earthquakes. A constant phase velocity Haskell-Thomson model was applied to generate synthetic *SH* seismograms at the surface using the accelerations recorded at 166 m. In the frequency band 0.10 to 10.0 Hz, we compared the filtered synthetic records to the filtered surface data. The onset of the *SH* pulse and the reflections from the interface at 30.5 m are clearly seen in both the synthetics and the recorded data. The synthetic records closely match the data in both amplitude and phase. The fit between the synthetic accelerograms and the data indicates that the seismic amplification at the surface is a result of the resonance of the surface layers and the contrast of the impedances (shear stiffness) of the near surface materials. The impedance contrast of the materials does not account for all of the amplification of the peak accelerations at the surface. The resonances of the layer system below 10 Hz contribute the most to this amplification. We find that a linear model predicts the soil response for frequencies up to 10 Hz. Material damping is added to the soil layers of the model in the form of a quality factor  $Q$ . The damping moderates the strong resonance effects by allowing energy to radiate into the half-space. The quality factor  $Q = 10$  is constant in this frequency range but does not accurately model the attenuation at frequencies above 10 Hz.

### INTRODUCTION

This work is a study of the competing site effects on earthquake ground motion: (1) attenuation in the near-surface material; (2) amplification induced by the lower impedance of the near-surface material; and (3) the resonance of an equivalent layer or layers on a half-space. The importance of this issue was dramatically emphasized in the events of 3 March 1985, Valparaiso, Chile,  $M_S$  8.1, (Celebi, 1987a) and 19 September 1985, Michoacan, Mexico,  $M_S$  8.1 (Anderson *et al.*, 1986; Celebi *et al.*, 1987; Mitchell, 1987). In both earthquakes the ground motion was amplified by the local near-surface site conditions. Seed *et al.* (1988) conducted a thorough investigation of the ground response at five sites on the soft clay layer of Mexico City. The authors used one-dimensional vertical wave propagation techniques to compute the ground response. The spectral characteristics of the computed and

recorded ground motions compared favorably. The authors concluded that the application of simple analysis methods can provide useful predictions of the site response. Bard *et al.* (1988) studied the amplification of earthquake motions in Mexico City due to the surface clay layer and the deep sediments. They employed one- and two-dimensional models in their calculations. The authors found that the deep sediments amplify seismic waves and that local two-dimensional heterogeneities in the clay layer can affect the ground motion.

These site effects are not limited to very large earthquakes. Similar amplifications were seen for the 2 May 1983, Coalinga,  $M_L$  6.5 (Mueller, 1986) and 24 April 1984, Morgan Hill,  $M_L$  6.1 (Celebi, 1987b) California earthquakes. In fact, a major conclusion drawn from the 1985 Valparaiso earthquake is that the weak ground motion could be used to identify the frequency ranges for which amplification occurs during the strong ground motion (Celebi, 1987a).

Given that so many metropolitan areas are built on alluvial fans or basins, the problem of site response is of major importance to any organization interested in earthquake hazards. Research in this area is concerned with describing amplification of an earthquake signal at a site, due to the lower impedance of the surface material and the resonance of surface layers, and attenuation of the signal, due to scattering and damping in the surface material. The site amplification and attenuation are competing effects; and either effect may dominate in a particular frequency band of the signal.

The problem of amplification/attenuation due to local site conditions has been addressed by both the seismological and engineering communities. The predominant method of study is to compare surface records taken on alluvium and bedrock during the same event. Most studies use weak motion earthquake data or data from distant nuclear explosions. An excellent review paper by Aki (1988) covers the classification of site conditions, empirical amplification factors, and analytical methods for site response predictions. Aki surveyed the available literature and found that weak-motion and strong-motion are reasonably well correlated at specific sites. Aki concluded that microzonation should be accomplished with empirical determination of site amplification factors, by performing regression analysis on earthquake data and comparing these factors with the parameters of the site such as sediment thickness, density, and shear-wave velocity. Rogers *et al.* (1985) collected weak motion data from Nevada nuclear test explosions in the Los Angeles region. The data were compared with geologic parameters that influence the site response, such as the void ratio and thickness of sediments. By clustering and correlating the site response and geologic data, they were able to predict the relative ground response of an area of the Los Angeles basin. The authors explained that the empirical method of using nuclear test data to predict site response is only valid if strong-motion and weak-motion amplification are assumed to be the same. They cited studies that support this assumption.

Mueller (1986) gave an exemplary review of state-of-the-art analysis of site effects on ground motion. The author studied the effects of site conditions on high-frequency ground motion from the Coalinga; 15 October 1979,  $M_L$  6.6, Imperial Valley; and 9 January 1982,  $m_b$  5.7, Miramichi events. He found that empirical methods gave better predictions of amplification than theoretical methods that used vertical seismic profiling data. Tucker and King (1984) looked at data from three sediment-filled valleys in the Garm region of the Soviet Union. They compared records taken on the surface of the sediments to records taken on rock outcroppings and found significant amplification. The site response was the same for ground accelerations from  $10^{-5} g$  to  $0.2 g$ . Joyner *et al.* (1981) analyzed strong-motion

records from the 1979 Coyote Lake event. They compared a record taken on 180 m of alluvium to one recorded on a bedrock outcropping. With a viscoelastic Haskell model of linear wave propagation, they modeled the site response to 5 Hz, finding no clear evidence of nonlinear soil response. Jarpe *et al.* (1988) examined weak- and strong-motion data from Coalinga, California. The records were taken on a soil site and a nearby bedrock site. Ground motions were amplified at the soil site by a factor of 2 to 3 compared to the bedrock. The authors found that the soil response was linear for frequencies up to 10 Hz and accelerations up to 0.7 *g*.

Borehole studies allow for the direct comparison of the response of the surface material to the response of the underlying bedrock. Seed and Idriss (1970) analyzed data at three different depths at Union Bay from a moderate earthquake and nuclear test explosions. The instruments were placed in the surface layer of peat and in two subsurface layers of clay and glacial till. Their lumped-mass model was used iteratively to represent the nonlinear material behavior. Records from the glacial till were the input base motion. The authors found good agreement between the data and their calculated motions. Joyner *et al.* (1976) studied weak motion data from a 186 m deep downhole array on the shore of the San Francisco Bay. The records were amplified at the surface by a factor of 4 or 5. The authors used a linear, viscoelastic Haskell plane-layer model. They found that  $Q = 16$  for the surface layer (bay mud) gave a best fit to the data. Surface accelerograms were computed by propagating the downhole record with the model. The authors concluded that "... our results provide further evidence that, under favorable conditions, simple, plane-layer models are capable of giving reasonably good approximations of the effects of local soil conditions on low-amplitude ground motion. Extension to the prediction of effects at high amplitude requires measures to take account of the nonlinear behavior of soil at high strain". Malin *et al.* (1988) recorded ultramicroearthquakes (with magnitudes less than 1.0) at a 500 m borehole at Oroville, California. They found evidence that a low  $Q$  value causes the attenuation of high frequency  $S$  waves near the surface. Redpath and Lee (1986) collected strong-motion data from the 58 m borehole at the Richmond Field Station. The peak horizontal surface acceleration from eight earthquakes was 0.01 *g*. Measurements of the attenuation gave an average  $Q$  of 12.5 for the soil layers. The authors concluded that surface motions computed with a linear, viscoelastic, plane-layer model were in good agreement with the earthquake data. Hauksson *et al.* (1987) analyzed data from a three-level 1500 m downhole array in the Baldwin Hills of Southern California. The records were generated by a single small earthquake ( $M = 2.8$ ) that occurred almost directly beneath the array. The authors found amplification factors of 4 for  $P$  waves and 9 for  $S$  waves. They also found low near-surface  $Q$  values.

Our work is almost unique in addressing the problem of local site amplification/attenuation in the United States. (Japan has a number of arrays of downhole and surface accelerometers that have recorded some of their larger earthquakes (Chen, 1985; Omori *et al.*, 1984).) With the exception of the Richmond Field Station operated by the University of California, Berkeley, which is distant from most earthquakes, this experiment is the first one that attempts to compare directly the strong ground motion in the basement to the ground motion at the surface. Two other downhole strong-motion experiments are currently in operation. An array of seismometers was installed in 1987 in a 5150 ft well at Parkfield, California (Malin *et al.*, 1987). In July of 1989, the accelerometers installed in boreholes at Lake Hemet, California (Sangas *et al.*, 1989) became operational.

Our work has provided direct evidence for the comparison of weak-motion to strong-motion; that is, we can test in a limited way the range over which linear

attenuation of seismic waves is valid. These *in situ* data directly demonstrate the effects of near-surface material on ground motion. The results of our analysis have important implications for nonlinear attenuation, microzonation using weak ground motion, resonances, and our general understanding of attenuation and amplification due to local site conditions.

#### DATA

The McGee Creek site (Fig. 1) is located in the Mammoth Lakes area of California ( $37^{\circ}32.9'N$ ,  $118^{\circ}48.7'W$ ). Three-component accelerometers and velocity transducers were installed at McGee Creek in November 1984. These instruments are at depths of 166 m, 35 m, and 0 m. Details of the installation of the instruments are described by Archuleta (1986). A schematic cross-section of the site instrumentation and geology is shown in Figure 2. (At this time the vertical velocity transducer at 35 m is the only velocity transducer operating correctly at depth. All of the accelerometers are currently operating.) The largest earthquakes recorded at McGee Creek are the 21 July 1986,  $M_L$  6.4, Chalfant Valley ( $37^{\circ}32.6'N$ ,  $118^{\circ}26.6'W$ , depth 11.2 km) (Maley *et al.*, 1986; Cockerham and Corbett, 1987) and the 23 November 1984,  $M_L$  5.8, Round Valley ( $37^{\circ}27.3'N$ ,  $118^{\circ}36.2'W$ , depth, 13.4 km) (Priestly *et al.*, 1988) events. Round Valley is at an epicentral distance of 22 km from the site. The Round Valley main shock was a left-lateral strike-slip event on a plane striking  $N30^{\circ}E$ . Peak accelerations from the main shock were around  $120 \text{ cm/sec}^2$ , with an amplification factor of approximately 5 from downhole to surface. The

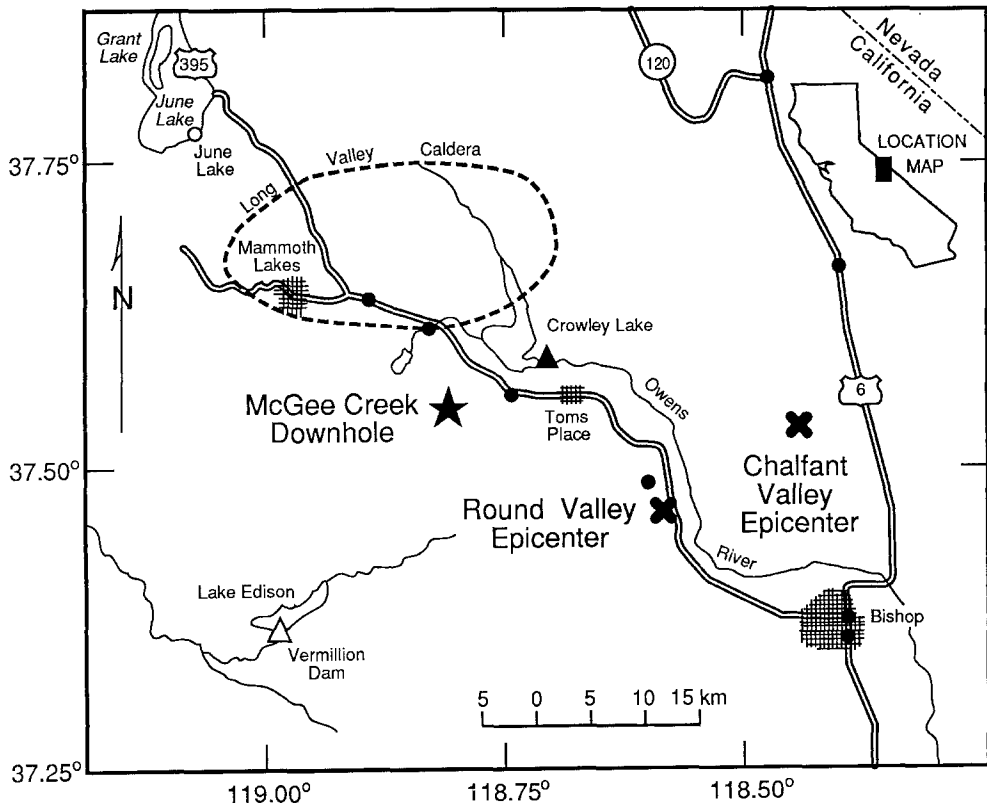


FIG. 1. The locations of the McGee Creek downhole and the epicenters of the Round Valley and Chalfant Valley events in the Mammoth Lakes region of California. Insert shows the area of interest relative to the State of California.

## MCGEE CREEK RECORDING SITE

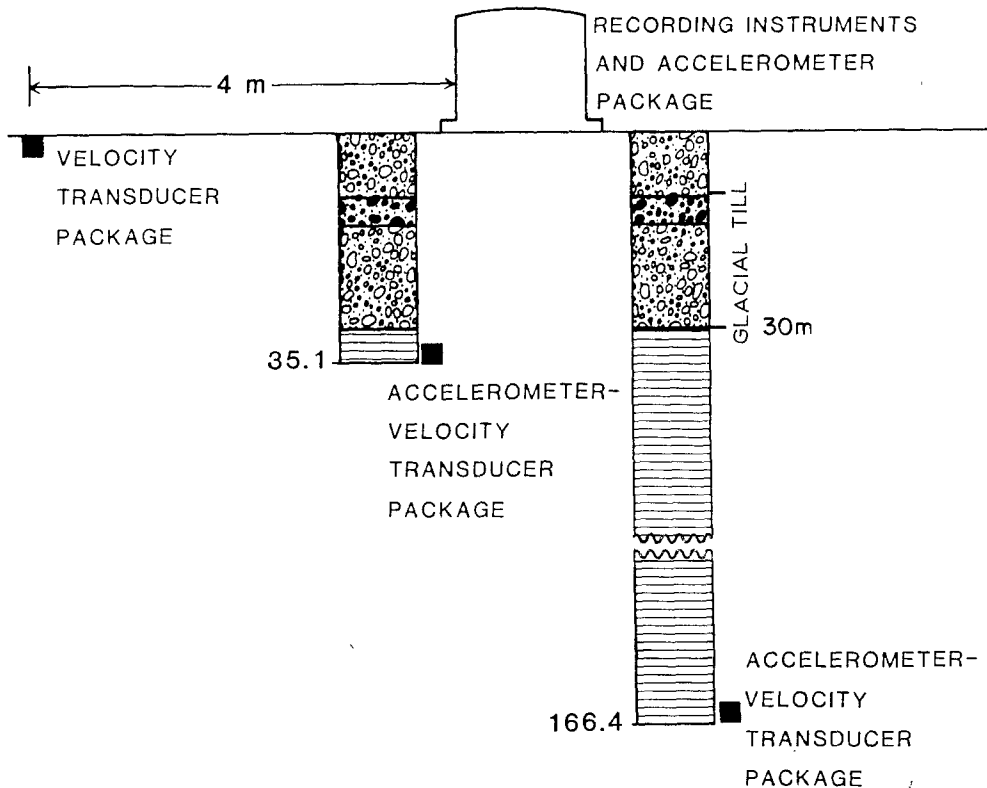


FIG. 2. The instrumentation and geology at McGee Creek. The first 30.5 m are glacial till. At depths from 30.5 m to 166.4 m the medium is hornfels. The instruments are located at 0 m, 35 m, and 166 m.

Round Valley accelerations from the three channels at each elevation are shown in Figure 3. The orientations of the downhole horizontal channels were determined with the Round Valley data, as described below. Chalfant Valley is at an epicentral distance of 32 km from McGee Creek. The Chalfant Valley main shock was a right-lateral strike-slip event on a plane striking N25°W and dipping 60° to the southwest. Peak accelerations from the Chalfant Valley earthquake were around 85 cm/sec<sup>2</sup> at the surface with considerably smaller amplitudes (about a factor of 5 less) at both 35 m and 166 m depths (Maley *et al.*, 1986). The Chalfant Valley data are shown in Figure 4.

Analyses of the strong-motion data from these events were performed with the USGS software package AGRAM (Converse, 1984). Fast Fourier transforms were performed on the rotated *SH* accelerograms at 0 m and 166 m for both earthquakes. The sampling rate of the data was 200 samples/sec. The accelerometers have a nominal natural frequency of 100 Hz. The data indicate that this frequency is around 75 Hz. Transforms were computed out to the Nyquist frequency of 100 Hz. For the Round Valley data, we had approximately 7 sec of record. The data were padded with zeros out to 10.24 sec, making the frequency interval of the transforms 0.0976 Hz. For the Chalfant Valley earthquake, we had exactly 20.48 sec of record and no padding was necessary. The frequency interval of the transforms was 0.0488 Hz. Transforms of the downhole records that were input to the model

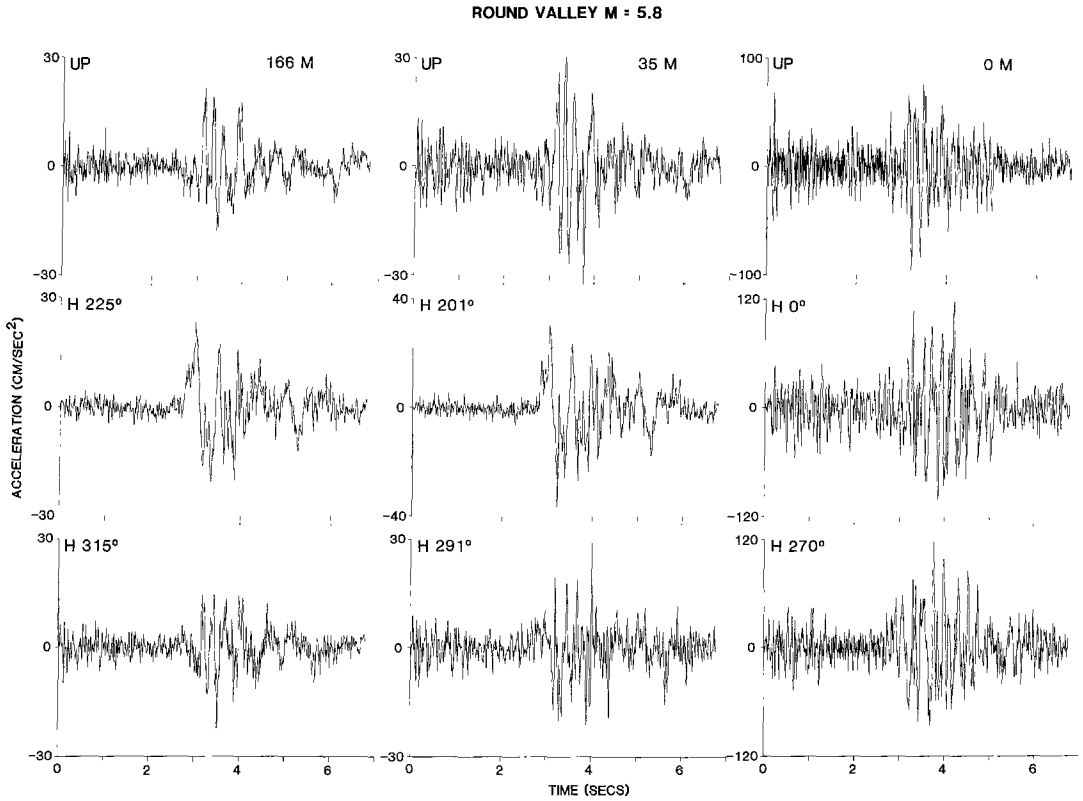


FIG. 3. The time histories of accelerations recorded at McGee Creek from the  $M_L$  5.8, 23 November 1984, Round Valley, California, earthquake. Three components of acceleration were recorded at 166 m, 35 m, and 0 m depths. For each depth, the components are arranged with the vertical component at the top and the two horizontal components beneath. The orientations, clockwise from North, of the horizontal components are indicated.

as base motion were not smoothed or tapered. Transforms of the seismograms that were used to compute amplitude spectral ratios were tapered but not smoothed. At each end of the time series, 10 per cent of the unpadded length was multiplied by a cosine half-bell taper. Seismograms at the surface, both recorded and computed, were lowpass-filtered to 10 Hz. In order to preserve the phase, we used a bi-directional Butterworth filter. The filter had two poles in each direction, giving the overall effect of a four-pole filter.

#### ANALYSIS

Our primary goal in this analysis was to take the accelerations recorded at 166 m, apply our knowledge of the material properties, and use linear wave propagation methods to produce a synthetic seismogram at the surface for comparison with the recorded data (Seale and Archuleta, 1988).

##### *Downhole Instrument Orientations*

The first step was to determine the orientations of the downhole horizontal components. When the downhole instruments were installed, the sense of their horizontal orientations was lost. The approximate orientations of the instruments were determined by comparing the horizontal strong-motion records with the location of an earthquake. For the McGee Creek site, we used the data from the Round Valley earthquake. The  $S$ -wave arrival for this event was very pronounced

CHALFANT VALLEY M = 6.4

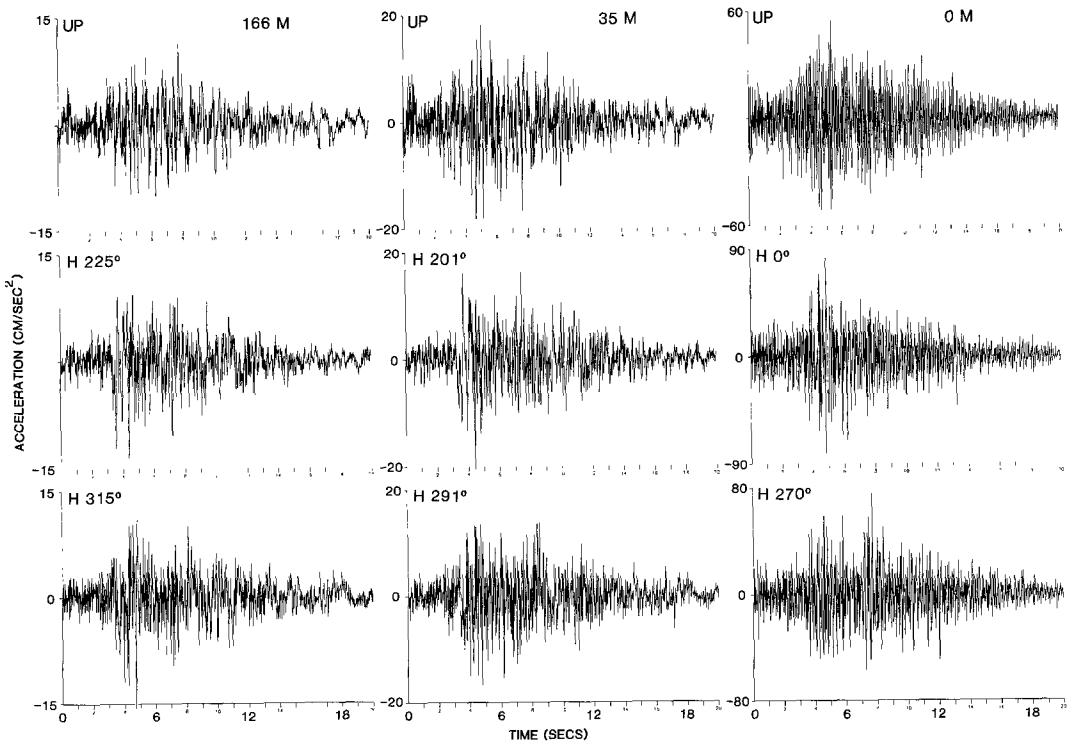


FIG. 4. The time histories of accelerations recorded at McGee Creek from the  $M_L$  6.4, 21 July 1986, Chalfant Valley, California, earthquake. The components are arranged as in Figure 3.

in the records from the downhole locations. At each depth, we calculated the orientation of maximum horizontal accelerations occurring over a window of time from the onset of the  $S$ -wave pulse. The direction of maximum horizontal accelerations should correspond to the direction of particle motion of the  $SH$  wave; and the direction of wave propagation is perpendicular to the direction of motion. By comparing the direction of wave propagation calculated from the instrument record to the angle of arrival of the earthquake, we estimated the orientations of the downhole instruments.

Each downhole instrument produced two perpendicular records of horizontal accelerations  $H_1$  and  $H_2$ , which were nominally assigned the directions "North" and "East." The components  $H_1$  and  $H_2$  were rigidly rotated by an angle  $\alpha$  (positive in the right-hand sense from  $H_1$ ) to produce the perpendicular components  $T_1$  and  $T_2$ :

$$\begin{aligned}
 T_1(t) &= H_1(t)\cos \alpha + H_2(t)\sin \alpha \\
 T_2(t) &= H_2(t)\cos \alpha - H_1(t)\sin \alpha.
 \end{aligned}
 \tag{1}$$

For each record,  $\alpha$  varied from 0 to  $2\pi$ . At a fixed  $\alpha$ , we computed  $T_1(t_i)$  at each discrete time in the time window. We then computed the sum of the squares (SSQ) of the  $T_1(t_i)$  at  $\alpha$ :

$$SSQ = \sum_{i=1}^n T_1(t_i) * T_1(t_i),
 \tag{2}$$

where  $n$  is the number of samples in the time window. The  $\alpha$  producing the largest SSQ was selected as the direction of  $SH$  motion. Notice that  $T_1(\alpha + \pi) = -T_1(\alpha)$  and thus there is an ambiguity of  $\pi$  in the choice of  $\alpha$ . The direction of  $SH$  motion must be inferred from the site geometry and the fault plane solution.

The Round Valley main shock data were uniquely well suited to the task of assigning orientations to the McGee Creek instruments. According to Priestly *et al.* (1987), the main shock was a left-lateral strike-slip event on a plane striking N30°E. Based on the location of the Round Valley earthquake (Robert Cockerham, personal comm.), we calculated that the azimuth of the arrival for the McGee Creek site was 301° clockwise (East) from North. (All angles are given clockwise from North.) The direction of  $SH$  motion was 31°. Thus there was an angle of approximately 90° between the site and the strike of the main shock. Since this was a nearly vertical strike-slip event, the signal arriving at McGee Creek was a maximum for  $SH$  with minimal  $SV$ - $P$  contribution.

For the Round Valley event, the onset of the  $S$ -wave pulse was approximately 2.7 sec from the beginning of the record. The initial pulse lasted about 0.5 sec. At 166 m, using time windows with lengths from 0.85 to 1.0 sec, the direction of  $SH$  motion was found to be 166° clockwise from  $H_1$ . This placed  $H_1$ , the “North” component of the instrument, at 225° and the “East” component at 315°. At 35 m, using time windows from 0.65 to 0.825 sec, the direction of  $SH$  motion was calculated to be 190° clockwise from  $H_1$ . This placed the “North” component at 201° and the “East” component at 291°. In Figure 5, we show the direction of arrival of the

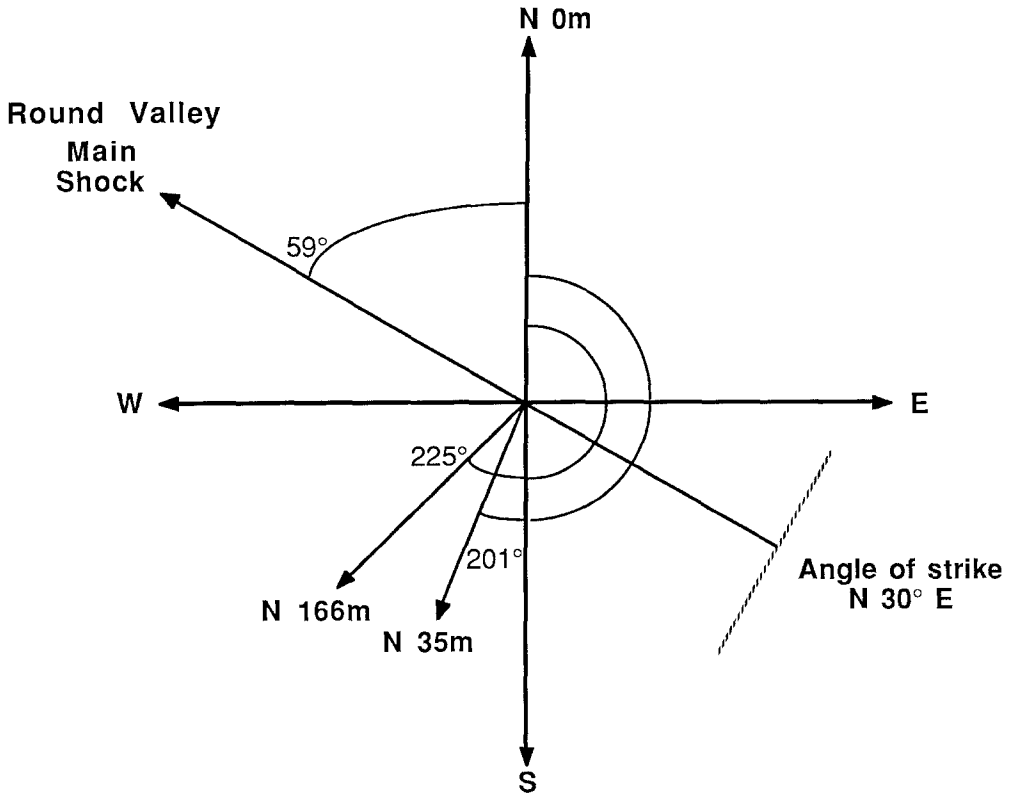


FIG. 5. A schematic diagram showing in plan view the radial direction of seismic waves from the Round Valley main shock (301° clockwise from North), the strike of the main shock, and the orientations of the “North” horizontal components at 166 m and 35 m.

Round Valley earthquake, the strike of the fault, and the directions of the "North" components at 166 m and 35 m.

Using these directions, we rotated the horizontal components of the acceleration records for the Round Valley earthquake into tangential (*SH*) and radial motion. Figure 6 shows the Round Valley *SH* accelerations at 0 m, 35 m, and 166 m, based on our orientations of the horizontal components. It is clear that we have good phase agreement between the records at 35 m and 166 m. In fact, after correcting for the velocity of the hornfels, these two records have a correlation of 89 per cent over 1.5 sec after the onset of the *SH* motion. (The calculation of the correlation coefficient is explained in detail below.) Figure 6 compares the surface *SH* accelerations with the *SH* accelerations downhole at the same scale. The amplification factor of the *SH* motions is 5.7.

The Chalfant Valley main shock was due East of the McGee Creek site. We calculated that the azimuth of arrival for the site was  $271^\circ$ . The Chalfant Valley earthquake was on a fault plane striking  $N25^\circ W$  and dipping  $60^\circ SW$ . Thus the rays leaving the fault were not emanating from a maximum for *SH* radiation. The direction of *SH* motion was  $1^\circ$ . The *S*-wave arrival was approximately 3 sec from the beginning of the record. Using the instrument orientations that we determined from the Round Valley earthquake, we rotated the horizontal acceleration components of the Chalfant Valley earthquake into tangential (*SH*) and radial motion. The  $H_1$  record at 166 m was rotated  $136^\circ$  clockwise for *SH*; and the  $H_1$  record at 35 m was rotated  $160^\circ$  clockwise. Figure 7 shows the Chalfant Valley *SH* accelerations at 0 m, 35 m, and 166 m. This figure compares the surface *SH* accelerations with the *SH* accelerations downhole. Again, there is amplification factor of 5.7 from downhole to surface. We also have good phase agreement between the

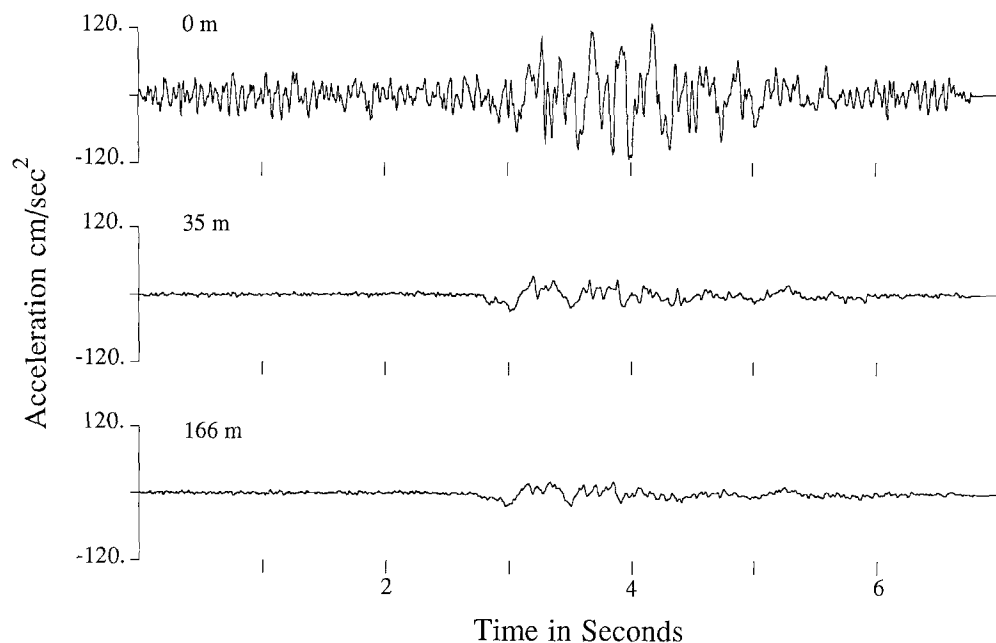


FIG. 6. A comparison of the Round Valley *SH* acceleration time histories at 166 m (bottom trace), 35 m (center trace), and the surface (top trace), plotted at the same scale to emphasize the amplification factor of 5.7. Based on the calculated orientations of the downhole horizontal components, the accelerograms were rotated into *SH*, horizontally polarized shear motion.

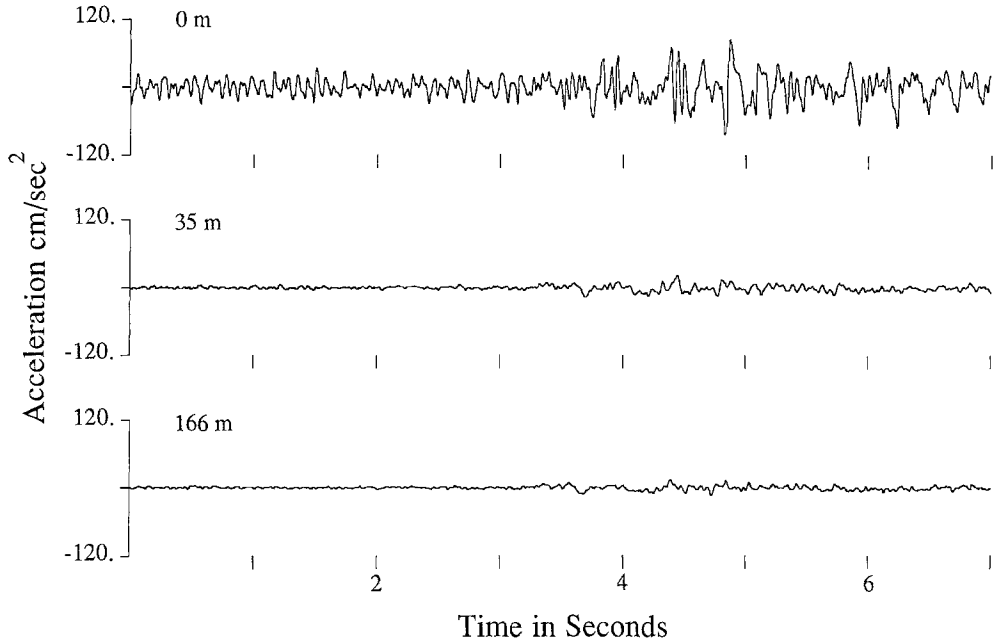


FIG. 7. A comparison of the Chalfant Valley *SH* acceleration time histories at 166 m (bottom trace), 35 m (center trace), and the surface (top trace), plotted at the same scale. Again note the amplification of 5.7.

records at 35 m and 166 m. After correcting for the velocity of the hornfels, these two records have a correlation of 82 per cent over 1.5 sec after the onset of the *SH* motion. The high correlations between the records at 35 m and 166 m, for both earthquakes, confirm the accuracy of the instrument orientations.

### *Spectral Ratios*

The next step in the analysis was to examine the spectral content of the *SH* acceleration data. We computed the spectral ratios by dividing the surface amplitude spectrum by the amplitude spectrum at 166 m at each frequency. Knowing that the McGee Creek site is the equivalent of two layers over a half-space (Fumal *et al.*, 1985), we expected that resonances would exist. The Fourier amplitude spectra of the *SH* accelerations at 0 m (upper plot) and at 166 m (lower plot) for the Round Valley event are shown in Figure 8. The ratio of these two spectra is shown in Figure 9. There are many resonant spikes at frequencies above 10 Hz; the two prominent spikes around 3 and 5 Hz are explicable from simple theory. Knowing the layer thicknesses and the material properties, we calculated the resonance frequencies of vertically traveling, unattenuated *SH* waves. The surface layer resonates at 5.2 Hz, the second layer at 9.7 Hz, and the two layers together at 3.4 Hz. The lower two frequencies remain the same for the *S*-wave phases discussed below. The Fourier amplitude spectrum of the *SH* accelerations at 0 m (upper plot) and at 166 m (lower plot) for the Chalfant Valley event are shown in Figure 10. Figure 11 shows the ratio of these two spectra. There are peaks around 3 Hz and 5 Hz, and there appears to be a peak between these two. The fact that the soil layers have resonance at the same frequencies for the two events suggests that the soil response is linear. We explore this in more detail below.

In our first attempt to model this spectral ratio we used the Haskell-Thomson propagation matrix for a vertically traveling *SH* wave (horizontal wavenumber

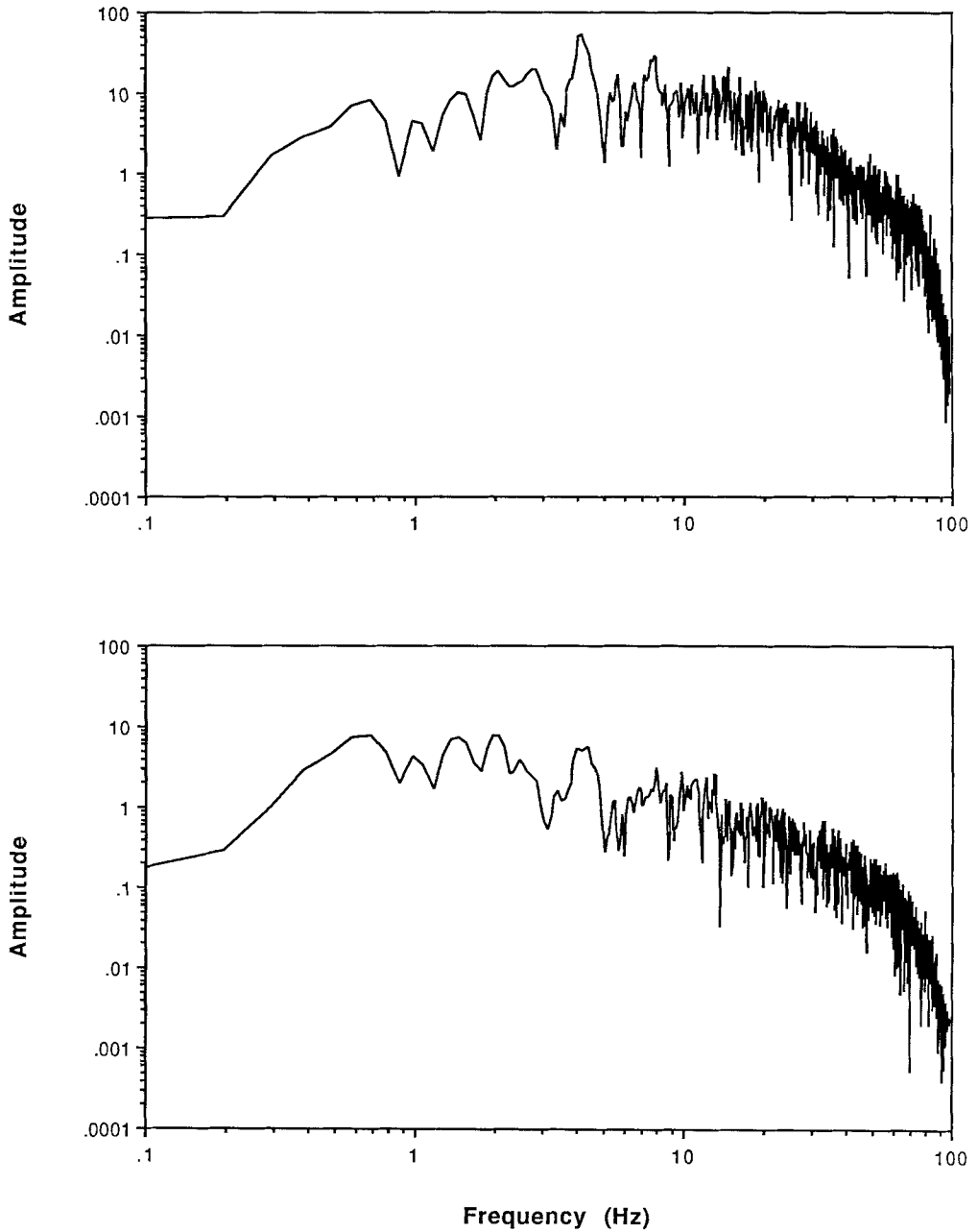


FIG. 8. The Fourier amplitude spectrum of the *SH* accelerations recorded from the Round Valley event. The upper plot is the spectrum of the record at 0 m; the lower plot is the spectrum of the record at 166 m.

$k = 0$ ). This matrix relates the anti-plane shear stress and displacement at the bottom of the layer to the stress and displacement at the top of the layer,

$$\begin{Bmatrix} v_2 \\ \frac{\tau_2}{\omega} \end{Bmatrix} = \begin{bmatrix} \cos \eta & \frac{-1}{\rho C_s} \sin \eta \\ \rho C_s \sin \eta & \cos \eta \end{bmatrix} \begin{Bmatrix} v_1 \\ \frac{\tau_1}{\omega} \end{Bmatrix}, \quad \eta = \frac{\omega h}{C_s}, \quad (3)$$

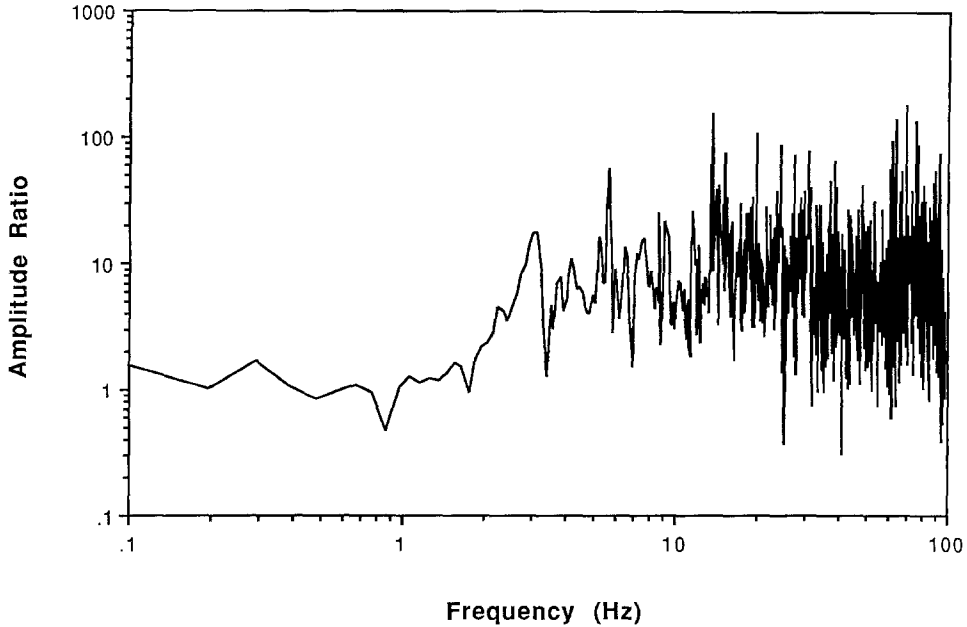


FIG. 9. The spectral ratio of the Round Valley *SH* accelerations at the surface to the *SH* accelerations at 166 m. Note the resonant peaks, particularly at about 3 and 5 Hz. Also note that the spectrum is fairly level for all frequencies greater than 20 Hz.

where  $v$  is the displacement,  $\tau$  is the shear stress,  $\omega$  is the frequency of the wave,  $h$  is the layer thickness, and  $C_s$  is the shear velocity of the layer. The subscripts  $_1$  and  $_2$  indicate the state variables at the top and bottom of the layer, respectively. These are the state variables at a fixed frequency  $\omega$  and wavenumber  $k$ . Our initial model consisted of three layers: glacial till from 0 m to 14 m ( $C_s = 330$  m/sec,  $\rho = 2.0$  g/cm<sup>3</sup>), glacial till from 14 m to 30 m ( $C_s = 620$  m/sec,  $\rho = 2.1$  g/cm<sup>3</sup>), and hornfels from 30 m to 166 m ( $C_s = 1320$  m/sec,  $\rho = 2.5$  g/cm<sup>3</sup>). The velocity data were obtained from logs at the McGee Creek site (Fumal *et al.*, 1985; Archuleta, 1986). When the three layer matrices are multiplied together, we obtain the anti-plane shear stress and displacement at 166 m in terms of the stress and displacement at 0 m. Since the shear stress at the surface is zero, we can directly relate the displacements.

$$v_{166} = \left[ \cos \eta_3 \cos \eta_2 \cos \eta_1 - \frac{\rho_1 C_{s1}}{\rho_2 C_{s2}} \cos \eta_3 \sin \eta_2 \sin \eta_1 - \frac{\rho_2 C_{s2}}{\rho_3 C_{s3}} \sin \eta_3 \sin \eta_2 \cos \eta_1 - \frac{\rho_1 C_{s1}}{\rho_3 C_{s3}} \sin \eta_3 \cos \eta_2 \sin \eta_1 \right] v_0 = K v_0 \quad (4)$$

The amplitude spectral ratio is obtained by computing the absolute value of the ratio of the displacements as a function of frequency.

$$\frac{|v_0(\omega)|}{|v_{166}(\omega)|} = \frac{1}{|K(\omega)|} \quad (5)$$

(Note that the spectral ratios for displacements and accelerations are the same, since differentiation by time twice introduces  $-\omega^2$  on both sides of equation (4).)

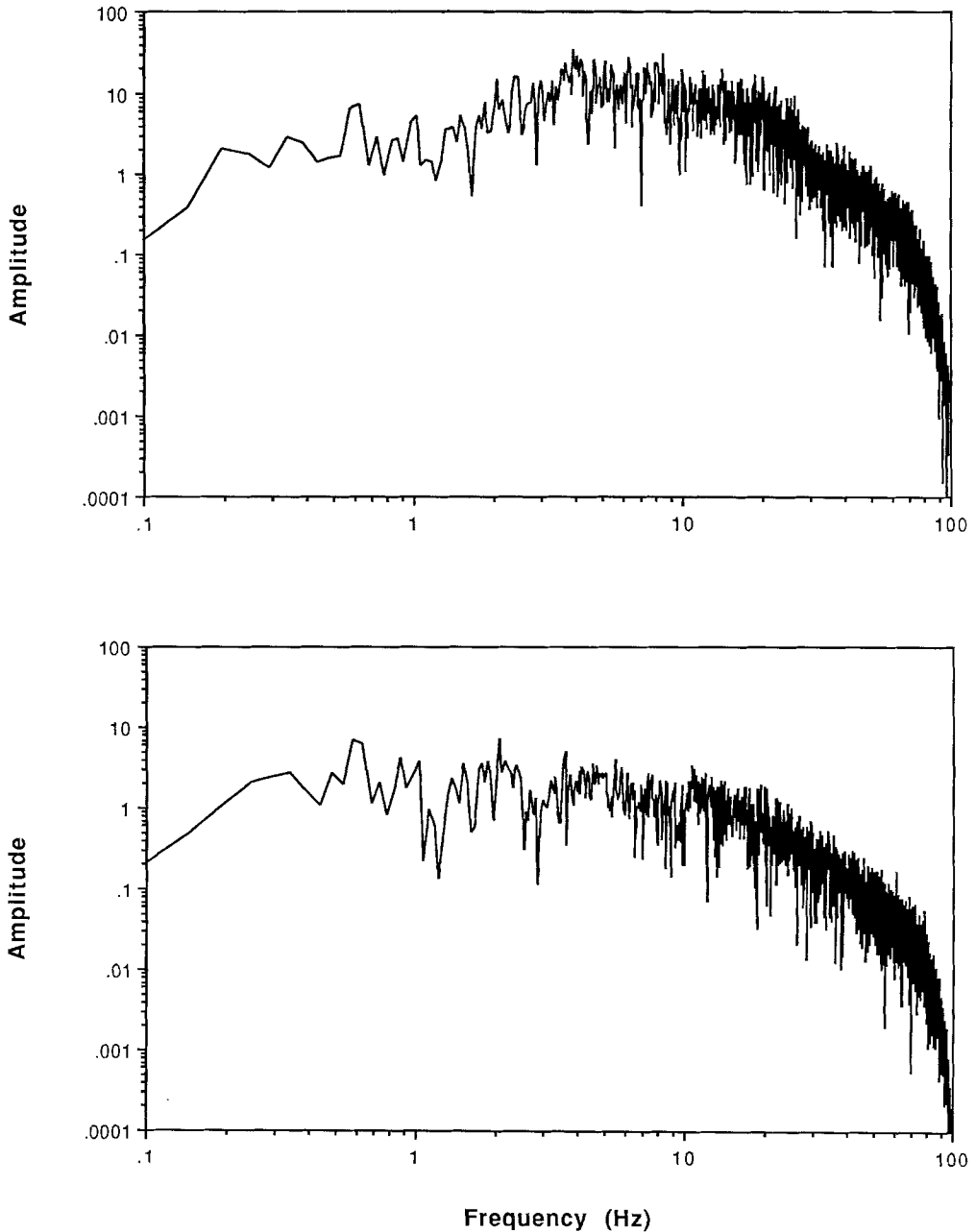


FIG. 10. The Fourier amplitude spectrum of the *SH* accelerations recorded from the Chalfant Valley event. The upper plot is the spectrum of the record at 0 m; the lower plot is the spectrum of the record at 166 m.

The spectral ratio calculated with this model is shown in Figure 12. The first two resonant peaks occur at 2 Hz and 4.5 Hz. These frequencies are lower than the data, an indication that our velocity model was not accurate. We determined that the shear velocity in the half-space (hornfels) was incorrect. To estimate the true velocity of the hornfels, we calculated the correlation coefficient between the *SH* acceleration records at 35 m and 166 m for both earthquakes. For *SH* acceleration

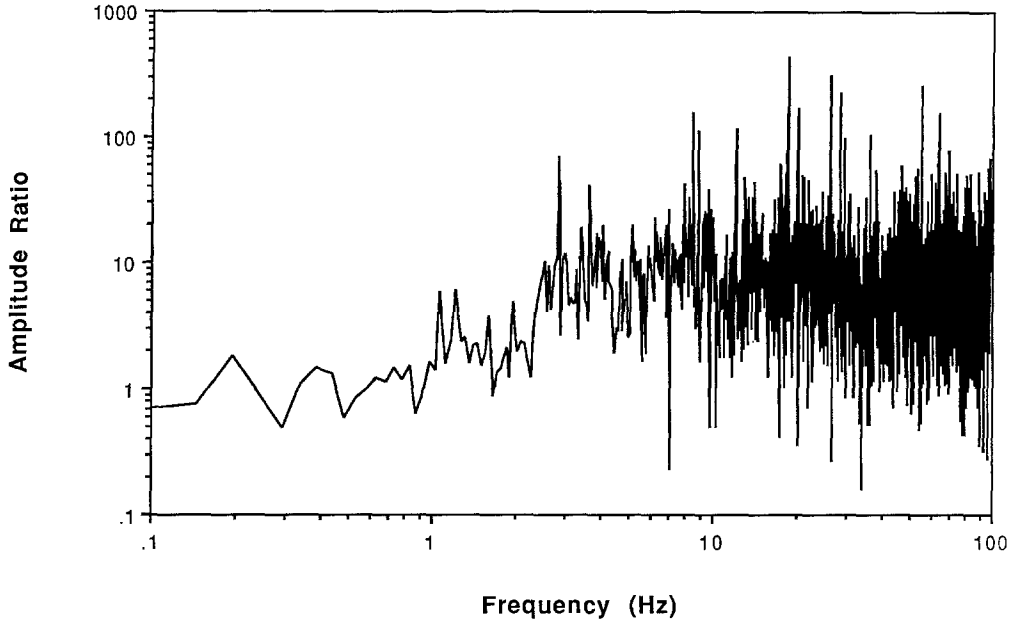


FIG. 11. The spectral ratio of the Chalfant Valley *SH* accelerations at the surface to the *SH* accelerations at 166 m.

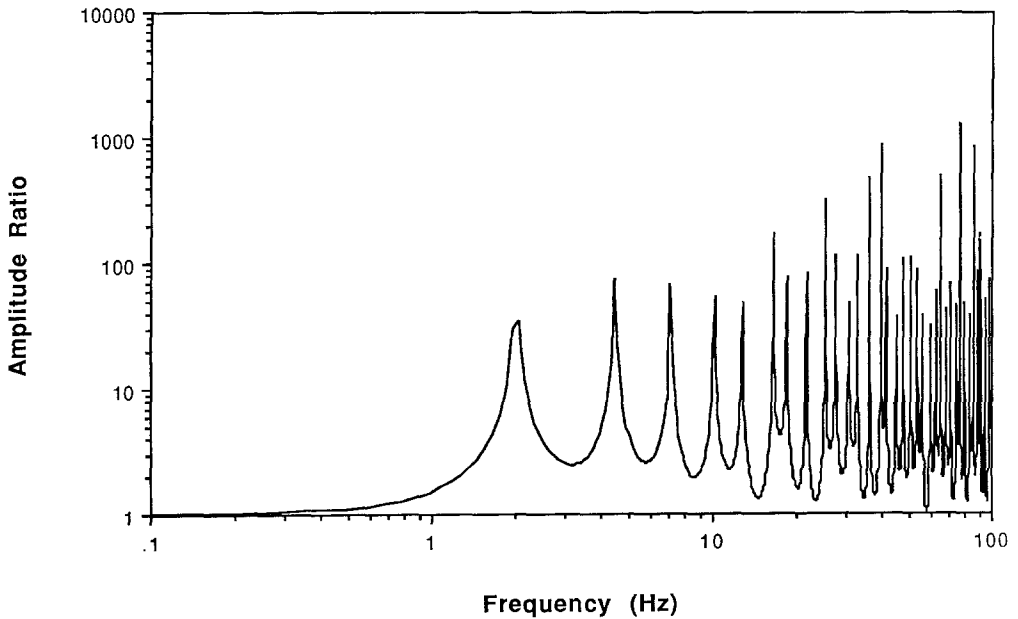


FIG. 12. The spectral ratio of the surface *SH* accelerations to the *SH* accelerations at 166 m, computed using the Haskell-Thomson propagator matrices for vertically incident *SH* waves. The model included the original material properties and no attenuation. Compared to the data, Figures 9 and 11, this spectral ratio has large amplitudes and resonant peaks located at the wrong frequencies.

records  $T_{35}(t)$  and  $T_{166}(t)$ , the sample correlation coefficient  $R$  is calculated as

$$R = \frac{n \sum_{i=1}^n T_{35}(t_i) T_{166}(t_i) - (\sum_{i=1}^n T_{35}(t_i)) (\sum_{i=1}^n T_{166}(t_i))}{\sqrt{n \sum_{i=1}^n T_{35}^2(t_i) - (\sum_{i=1}^n T_{35}(t_i))^2} \sqrt{n \sum_{i=1}^n T_{166}^2(t_i) - (\sum_{i=1}^n T_{166}(t_i))^2}}, \quad (6)$$

where  $n$  is the number of samples in the time interval. The correlation was computed over 1.5 sec after the arrival of the  $S$  wave. The records at 35 m were shifted in time until the correlation reached its maximum. The vertical distance between the stations (131 m) was divided by the time lag to estimate the velocity. For the Round Valley earthquake, the correlation coefficient was  $R = 0.89$  when the record at 35 m lagged by 0.045 sec and 0.050 sec. This gave shear velocities of 2911 m/sec and 2620 m/sec. We tried several different values of  $C_s$  in the range of 2620 m/sec to 2911 m/sec for the hornfels in the model. The best fit to the data was obtained with a shear-wave speed of 2800 m/sec. For the Chalfant Valley earthquake, the correlation reached its maximum  $R = 0.82$  when the time shift was 0.040 and 0.045 sec. With a velocity  $C_s = 2800$  m/sec, the Poisson's ratio is  $\nu = 0.28$ .

In the spectral ratio of the vertically propagating  $SH$  wave, the amplitudes of the resonant peaks were much too large, indicating a need to add material damping to the model. Hysteretic damping in the form of a complex shear modulus was added:

$$G^c = G(1 + 2i\beta), \quad (7)$$

where  $G$  is the shear modulus of the layer,  $\beta$  is the ratio of critical damping, and  $i = \sqrt{-1}$ . A damping ratio of  $\beta = 0.05$  (5 per cent of critical) in the upper two layers and no damping in the hornfels gave the best fit to the data. Quality factor  $Q$  is inversely proportional to damping,

$$Q = \frac{1}{2\beta}, \quad (8)$$

so that  $\beta = 0.05$  gives  $Q = 10$ .

Our next step in the analysis was to improve our model by considering  $SH$  waves with incidence angles other than  $0^\circ$ . Because the Round Valley earthquake and the McGee Creek site are both within the Sierra granitic batholith, we assumed a straight line ray path. The straight line ray path incidence angle for the Round Valley earthquake was approximately  $56^\circ$ , measured from the vertical. From the Chalfant Valley earthquake, the straight line ray path incidence angle was  $71^\circ$ . For an  $SH$  wave traveling an angle  $\theta$ , the horizontal phase is calculated as

$$c = \frac{C_s}{\sin \theta}. \quad (9)$$

For Round Valley, the angle of  $56^\circ$  gives a horizontal phase velocity of 3377 m/sec. The angle of  $71^\circ$  gives a phase velocity of 2960 m/sec. (At these phases, the angle of refraction in the top layer is approximately  $6^\circ$ . Thus the spectral ratios for the two angles of incidence are similar. This phenomenon is discussed by Joyner *et al.* (1976).)

Our model then included material damping and the new shear velocity in the hornfels. We applied the Haskell-Thomson propagation matrix for a wave with constant phase

$$\left\{ \begin{array}{c} v_2 \\ \tau_2 \\ k \end{array} \right\} = \left[ \begin{array}{cc} \cosh k\xi h & \frac{-1}{G^c \xi} \sinh k\xi h \\ -G^c \xi \sinh k\xi h & \cosh k\xi h \end{array} \right] \left\{ \begin{array}{c} v_1 \\ \tau_1 \\ k \end{array} \right\}, \quad \xi = \sqrt{1 - \left( \frac{\omega}{kC_s^c} \right)^2}, \quad (10)$$

where now the shear modulus and shear velocity are complex. We again multiplied the three layer matrices to obtain displacements at 166 m in terms of displacements at 0 m. The material parameters of the model were adjusted to obtain the best fit to the data. We found that in the upper 14 m a shear velocity of 290 m/sec gave the best fit to the Round Valley data. We also found that adding a  $\beta$  of 5 per cent ( $Q = 10$ ) in the upper two layers was necessary to obtain the correct spectral amplitudes. Our best estimates of the material parameters at McGee Creek are shown in Figure 13.

Figures 14 and 15 show the spectral ratios of the data (solid lines), plotted with the spectral ratios of the constant phase models for the Round Valley and Chalfant Valley earthquakes (dashed lines), from 0.10 to 20 Hz, respectively. Comparisons of the synthetic spectral ratios with the data show an immediate discrepancy. The spectral ratios of the model have a pronounced attenuation of the spectral amplitudes for frequencies above 10 Hz, much more severely than is seen in the data. Yet for frequencies less than 10 Hz, the fit between the data and the model is quite good. The model has matched the first resonant peak in amplitude and location (around 3 Hz). It has a higher mode, around 7.5 to 8 Hz, that is also seen in the data. The model is missing the 5 Hz peak, which is clearly seen in the Round Valley data.

#### Material Strains

We were interested to know the order of magnitude of the strains developed at the surface during these earthquakes. If the strains were on the order of  $10^{-4}$ , then the soil response remained linear. Spudich and Cranswick (1984) proposed a method for estimating the size of strains when ground motions and phase velocity are known. If  $v$  is the anti-plane displacement of a plane  $SH$  wave traveling with

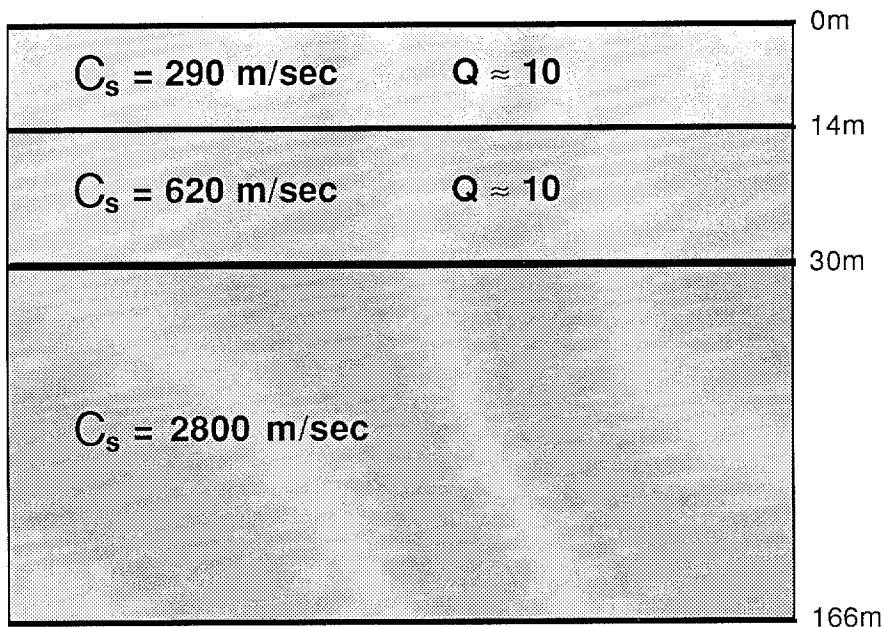


FIG. 13. The material parameters that are most consistent with the data, based on modeling the spectral ratio of the Round Valley data. The major changes are the shear-wave velocities of 2800 m/sec in the hornfels and 290 m/sec in the upper 14 m, compared with 1320 m/sec and 330 m/sec, respectively, which were obtained from logs.  $Q = 10$  in the upper 30 m, which was not previously measured.

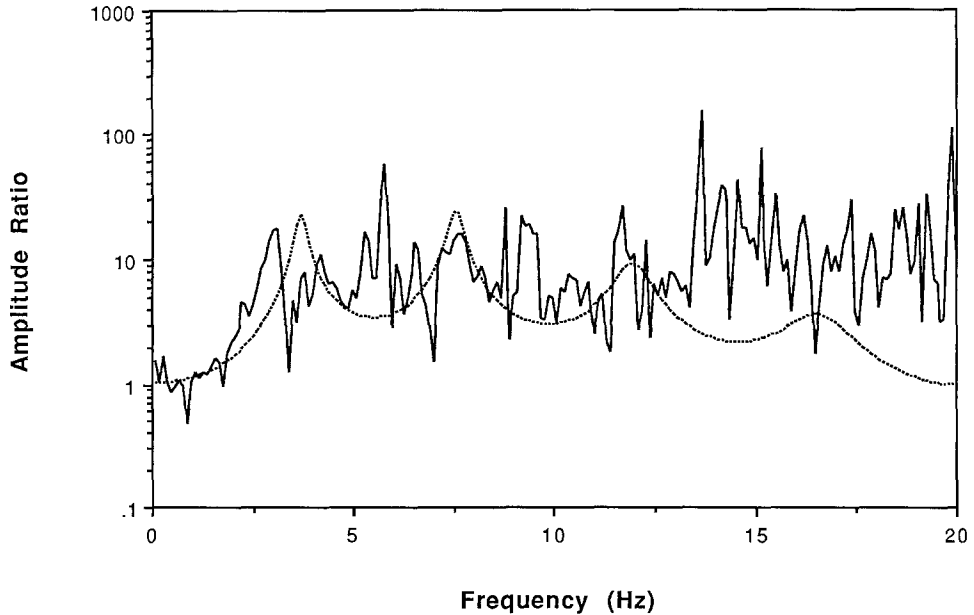


FIG. 14. The spectral ratio of the synthetic *SH* accelerogram at 0 m depth to the *SH* accelerogram at 166 m for the Round Valley earthquake (dashed line), from 0 to 20 Hz. Compared with the data (solid line), the amplitude and position of two of the resonant peaks below 10 Hz are in excellent agreement. Above 10 Hz the synthetic spectral ratio shows a systematic decrease due to *Q*. This decrease is not observed in the data.

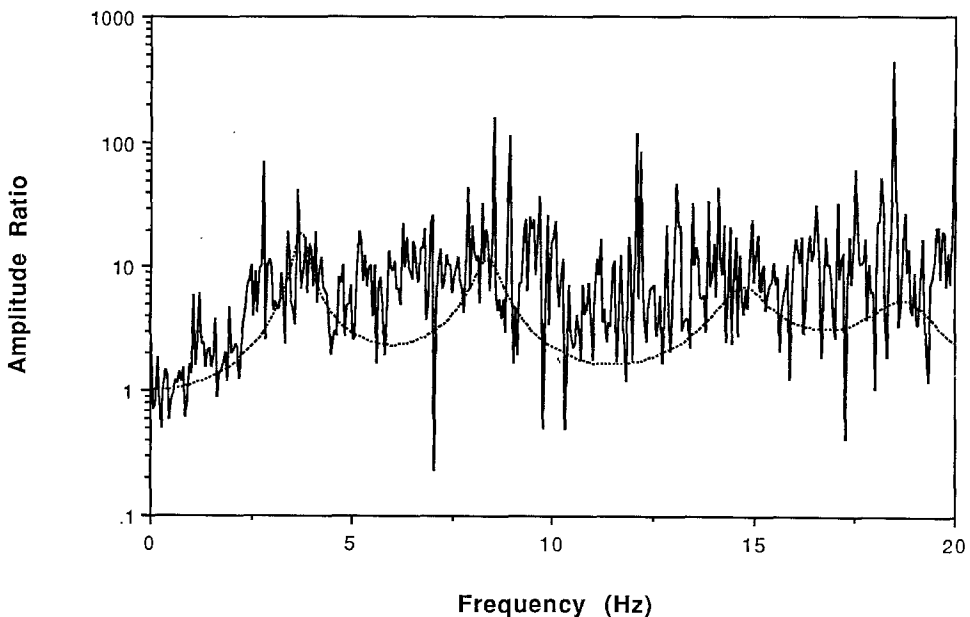


FIG. 15. The spectral ratio of the synthetic *SH* accelerogram at 0 m depth to the *SH* accelerogram at 166 m for the Chalfant Valley earthquake (dashed line), from 0 to 20 Hz. Compare with the data (solid line). Again, the synthetic spectral ratio shows a systematic decrease at frequencies above 10 Hz due to *Q* not observed in the data.

horizontal phase velocity  $c$ , then the anti-plane shear strain  $\gamma$  is equal to the particle velocity divided by the phase velocity,

$$\gamma = \frac{\partial v / \partial t}{c}. \quad (11)$$

An estimate of the shear strain is the maximum particle velocity divided by the phase velocity. For each earthquake, we used the phase velocity of the straight line ray path described above. For Round Valley and Chalfant Valley, the phase velocities are 3377 m/sec and 2960 m/sec, respectively. For the Round Valley event, the maximum velocities at the surface were 4.475 cm/sec and 3.968 cm/sec on the horizontal components. Taking the square root of the sum of the squares of the maximum velocities and dividing by the phase velocity gives an upper limit on the shear strain of  $1.8 \times 10^{-5}$ . For the Chalfant Valley event, the maximum velocities at the surface were 2.742 cm/sec and 2.377 cm/sec. The upper bound on the shear strain is  $1.2 \times 10^{-5}$ . Since these strains are small in magnitude, we can model the ground response with a linear wave propagation method.

### *Synthetic Surface Accelerograms*

Because the spectral content of the constant phase model fit the data well up to 10 Hz, we proceeded to calculate synthetic seismograms at the surface. Our method was to take the acceleration record at 166 m and apply the Haskell-Thomson matrices to compute the accelerations at the surface. The FFT of the record at 166 m was used. At each frequency  $\omega$ , from 0 to 100 Hz, the transform of the accelerations at 166 m ( $\ddot{v}_{166}(\omega)$ ) was divided by the constant phase Haskell-Thomson coefficient, to yield the acceleration at 0 m:

$$\ddot{v}_0(\omega) = \frac{\ddot{v}_{166}(\omega)}{K(\omega)}. \quad (12)$$

We then applied an inverse FFT to the complete record of acceleration at the surface in order to produce a synthetic accelerogram in the time domain.

Our method of applying the Haskell-Thomson matrices differs from that used in standard engineering practice in that we have a downhole record as input. Typically, only motions recorded on a bedrock outcropping are available (Seed *et al.*, 1988). With these motions, the amplitudes of the upgoing *phases* are calculated and then used as base motions in an analysis of soil layers resting on the same bedrock. By applying the stress-free boundary condition at the surface, one can obtain the amplitudes of the downgoing phases and then the motions at each layer interface. With the downhole record, we have the complete motions in the bedrock. After applying the surface boundary condition, we compute the motions at the layer interfaces directly. The record from 166 m contains the upgoing and downgoing phases. It is not necessary to extract the upgoing phases for the analysis.

A simple example serves to illustrate some aspects of this model. We applied a single displacement pulse at 166 m depth and at  $t = 2$  sec. The pulse has amplitude equal to 1 and horizontal phase velocity of 3377 m/sec. The pulse and the resulting surface motion are shown in Figure 16. The arrival of the pulse at the surface is delayed by the travel time of this phase to the surface. The effect of the attenuation can be clearly seen. The reflections off the layer interfaces are damped out in a few

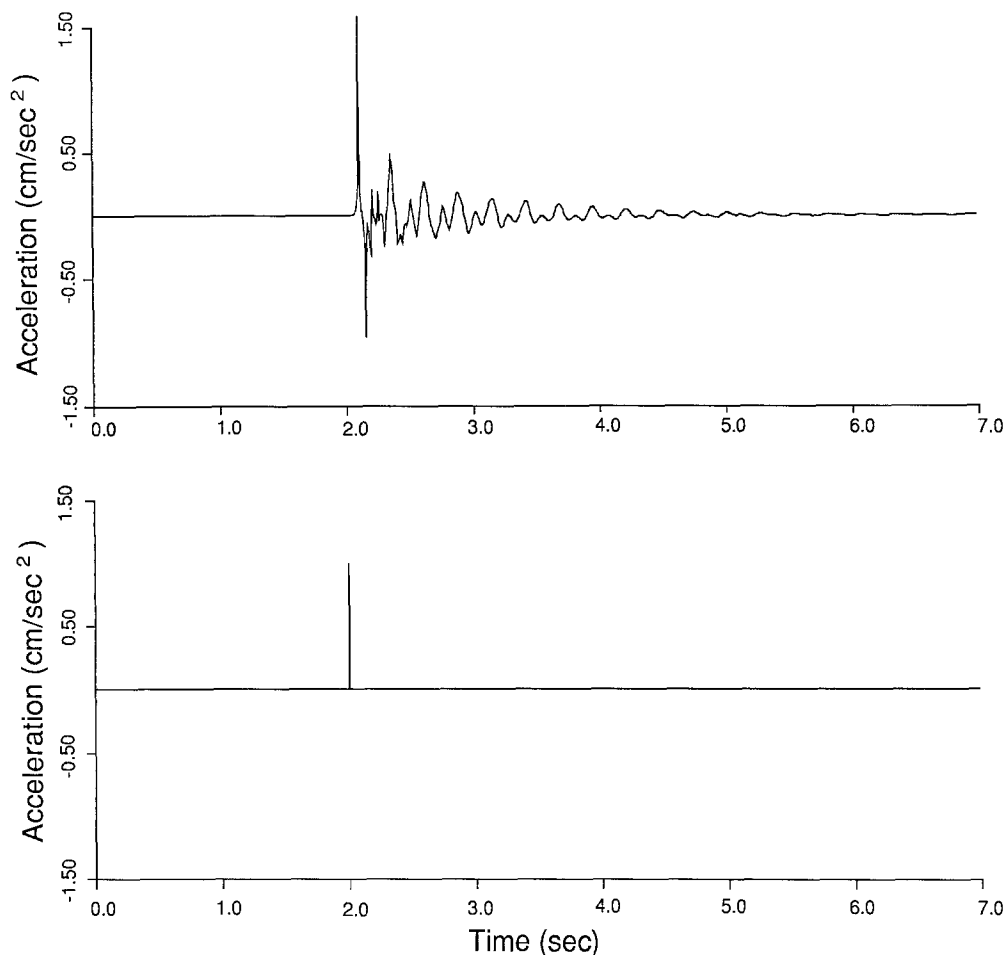


FIG. 16. A displacement pulse with amplitude of 1.0 and horizontal phase velocity of 3366 m/sec is input to the Haskell-Thomson model at 166 m (bottom trace). The resulting displacements at the surface (top trace) have an amplification of 1.5.

seconds. The damping also has an effect on the amplification of the pulse. The amplitude of the pulse at the surface is approximately 1.5. The calculation of transmission coefficients of this phase, considering the material parameters of the model and the free surface effect, gives an amplification factor of 4.1 at the surface. The material damping in the surface layers ( $Q = 10$ ) reduces the amplification due to the impedance contrast to approximately 40 per cent of its value.

The spectral ratios of Figures 14 and 15 indicated that we would not have good results for our synthetics in the higher frequencies. Thus the acceleration records at the surface and the synthetics were lowpass-filtered to 10 Hz. In Figure 17 we plot the synthetic *SH* surface acceleration time history (dashed line) with the Round Valley data (solid line), both lowpass-filtered to 10 Hz. Although frequencies above 10 Hz have been filtered from the data, the acceleration amplitudes are still about 79 per cent of the unfiltered data. The amplification factor of peak acceleration from downhole to surface in this frequency range is 6.0. The agreement in amplitude, phase, and duration is quite remarkable, especially considering that we are modeling the data up to 10 Hz with a single phase. Careful inspection of the data shows an

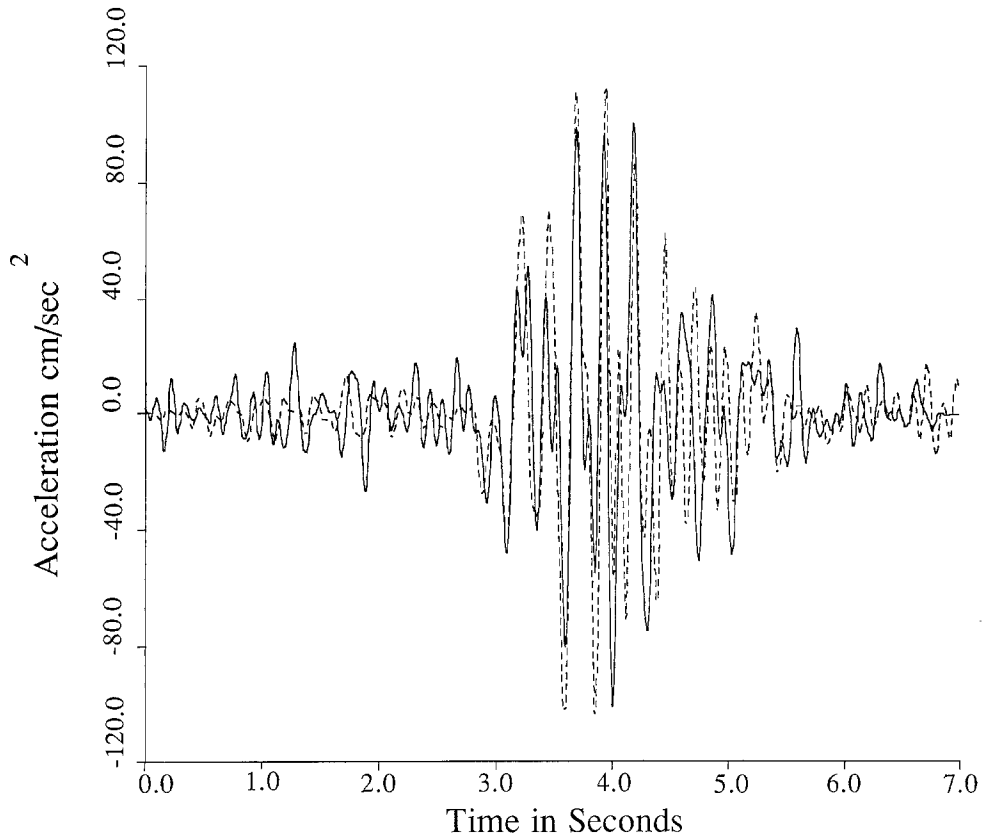


FIG. 17. The Round Valley synthetic *SH* accelerogram (dashed line), computed using the Haskell-Thomson matrices to propagate the *SH* accelerations at 166 m to the surface, and then lowpass-filtered to 10 Hz. The material parameters shown in Figure 13 and an incidence angle of  $56^\circ$  at 166 m are used in the constant phase model. The actual Round Valley *SH* accelerogram (solid line), recorded at the surface, is lowpass-filtered to 10 Hz for comparison. Note the similarities in peak amplitudes, phase, and duration. The data still show a reverberation that does not appear in the synthetic.

extra beat that interferes with the signal, constructively and destructively. In Figure 18, we plot the synthetic *SH* accelerogram with the Chalfant Valley data. The peak acceleration is 77 per cent of the unfiltered data and the amplification factor is approximately 6.0. Again, the fit between the data, in phase and amplitude, is excellent. Our simple Haskell-Thomson model gave excellent results for both earthquakes, even though they were in different locations and at different depths.

#### DISCUSSION

Our work can be compared, for site location and methodology, to the downhole studies described above. The major difference between our study and earlier ones is that they all have used weak motion data exclusively. In the work by Seed and Idriss (1970), the Union Bay site was unusual compared to McGee Creek. The deepest instrument was placed not on bedrock but in a layer of glacial till. The upper clay amplified the earthquake and nuclear test data. The acceleration amplitudes recorded on the surface layer of peat were half as large as those recorded in the glacial till for the earthquake, but were four to six times larger for the nuclear test data. Peat is an organic, fibrous material that obviously exhibits nonlinear behavior. The quasi-static model was able to capture this behavior reasonably well.

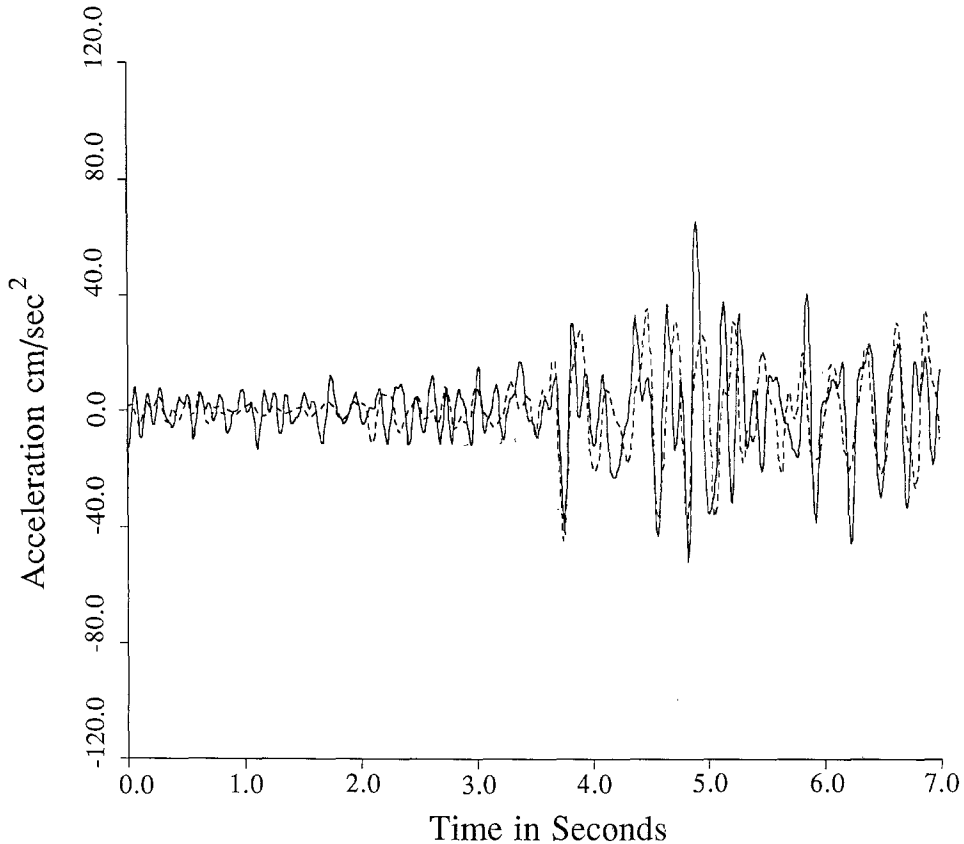


FIG. 18. The Chalfant Valley synthetic *SH* accelerogram (dashed line), computed using the Haskell-Thomson matrices to propagate the *SH* accelerations at 166 m to the surface, and then lowpass-filtered to 10 Hz. The material parameters shown in Figure 11 and an incidence angle of  $71^\circ$  at 166 m are used in the constant phase model. The actual Chalfant Valley *SH* accelerogram (solid line), recorded at the surface, is lowpass-filtered to 10 Hz for comparison. As in Figure 17, note the similarities in peak amplitudes, phase, and duration. These data also show a reverberation that does not appear in the synthetic.

Many of these works, as discussed above, have described low  $Q$  values in surface materials. The Baldwin Hills site where Hauksson *et al.* (1987) did their downhole study had large surface amplification of *S* waves, as did McGee Creek. The authors also found evidence for low  $Q$  values near the surface. Joyner *et al.* (1976) used a Haskell plane-layer model similar to ours. Their earthquake data showed amplification at the surface relative to the bedrock at 186 m. They also found that low  $Q$  values near the surface gave the best fit to the data. Their synthetic surface seismograms matched the data well in amplitude and frequency content.

Using the Round Valley data, the material parameters were adjusted by comparing results obtained from the model with this data. The shear velocity of the hornfels was adjusted after correlating the *SH* records at 35 m and 166 m. The value of 1320 m/sec, calculated from logs, was too small. The McGee Creek site was logged before the pneumatic shear-wave generator (Liu *et al.*, 1988), which gives more accurate results, was in use by the USGS. Because of the strong impedance contrast at 30.5 m, the first arrival of the *S* wave, which is generated at the surface during the logging of the hole, is very weak in the hornfels. Consequently, a stronger secondary arrival was originally interpreted as the *S* wave, leading to a

lower shear velocity. The value of 2800 m/sec was chosen because: (1) it was in the range suggested by the correlation of the downhole records and (2) it gave the best fit to the data. The shear velocity of the upper 14 m was changed to 290 m/sec from 330 m/sec. The 12 per cent change was chosen because it improved the fit of the model to the data. Damping of 5 per cent ( $Q = 10$ ) in the upper two layers gave the best fit of the amplitudes of the resonant peaks in the model spectral ratio to the amplitudes of the resonant peaks of the Round Valley data spectral ratio, for frequencies up to 10 Hz. In the time domain, the acceleration amplitudes of the model also match the Round Valley data well. Good results were obtained with the model and the Round Valley data for frequencies up to 10 Hz.

The model that we developed with the Round Valley data was used without modification to compute the surface strong-motion records from the Chalfant Valley earthquake. We simply calculated the phase of the straight line ray path and rotated the horizontal components into *SH* motion. No adjustments were made to the orientations of the downhole instruments or to the material parameters of the model. Using this phase and the data as the input to the model, we computed the spectral ratio and synthetic surface seismograms. The accuracy of our model is established by the fact that excellent results, in phase and amplitude, were obtained with the independent second data set.

Our results show that the linear model does capture the amplification of strong-motion in surface layers up to 10 Hz. We know that the motions in the surface layer remain linear, since the maximum shear strains are on the order of  $10^{-5}$ . Close to 80 per cent of the peak acceleration is accounted for by frequencies less than 10 Hz. In the surface seismograms, we have not been able to identify the source of the additional phase that appears in the data. It could be *P*-wave energy, as it seems to be traveling at about twice the speed of the principal phase. It could also be the resonance at 5 Hz, which appears in the spectral ratios of the data but not in the model.

The issue of frequency-dependent  $Q$  for frequencies greater than 10 Hz needs to be investigated. The constant  $Q$  of our model introduces a trend in the spectral ratio above 10 Hz that does not exist in the data. This implies that the attenuation mechanism in the material may depend on frequency; however, this dependence will lessen the attenuation for higher frequencies. The higher frequencies, i.e., the shorter wavelengths, may be more strongly affected by material inhomogeneities and the assumption of a single phase is no longer valid. Apparently this effect does not lead to more attenuation. While scattering is likely to attenuate the higher frequency signal, it is not included in a Haskell-Thomson method. The high correlation between the records at 35 m and 166 m after the arrival of the *S* wave indicates that most of the energy remains in the surface layers. The energy is resonating in the upper layers and being attenuated by scattering and material damping.

Clearly the amplification of accelerations at the surface is due to the resonance of the upper two layers and the impedance contrast of the surface material to the hornfels. Our analysis indicates that the surface response is dominated by the resonance of the upper two layers. Due to the impedance contrast and free surface effect, and in the absence of damping, the amplification factor from downhole to surface is approximately 4 for the two phases studied. In the presence of 5 per cent material damping in the surface layers, the mathematical example of a pulse applied at 166 m depth in the Haskell-Thomson model results in an amplification of only 1.5 at the surface. Yet, in the data, the peak accelerations at the surface are

5.7 times greater than those recorded downhole. When we input the downhole record as the base motion in the model, correct amplitudes are obtained at the surface. This indicates that the major cause of the amplification seen at the surface is the resonance of the signal in the surface layers. This resonance more than compensates for the attenuation due to low  $Q$ .

#### ACKNOWLEDGMENTS

This research is supported by the Office of Nuclear Regulatory Research, U.S. Nuclear Regulatory Commission Grant No. NRC-G-04-85-004. The U.S. Forest Service provided the McGee Creek site. We thank the USGS, especially Gerald Brady, Peter Mork, and Ed Etheridge for processing the data and maintaining the instruments and April Converse for helping with AGRAM. We also thank C. B. Crouse and an anonymous reviewer for their helpful comments on the manuscript. Figures 2, 3, 5, 13, and 17 and portions of the text are reproduced with the permission of the American Society of Civil Engineers.

#### REFERENCES

- Aki, K. (1988). Local site effects on ground motion, *Earthquake Engineering and Soil Dynamics II—Recent Advances in Ground-Motion Evaluation, Proc. of the A.S.C.E. Specialty Conference*, June 27–30, Park City, Utah, 103–155.
- Anderson, J. G., P. Bodin, J. N. Brune, J. Prince, S. K. Singh, R. Quaas, and M. Onate (1986). Strong ground motion from the Michoacan, Mexico, earthquake, *Science* **233**, 1043–1049.
- Archuleta, R. J. (1986). Downhole recordings of seismic radiation, *Earthquake Source Mechanics, Geophys. Monograph 37 (Maurice Ewing 6)*, S. Das, J. Boatwright, and C. Scholz (Editors), American Geophysical Union, Washington, D.C., 319–329.
- Bard, P.-Y., M. Campillo, F. J. Chavez-Garcia, and F. Sanchez-Sesma (1988). The Mexico earthquake of September 19, 1985—a theoretical investigation of large- and small-scale amplification effects in the Mexico City valley, *Earthquake Spectra* **4**, 609–633.
- Celebi, M. (1987). Distant resonance effects of the earthquake—a preliminary study, *The Morgan Hill, California, Earthquake of April 24, 1984*, S. W. Hoose (Editor), U.S. Geological Survey Bulletin 1639, Washington, D.C., 105–110.
- Celebi, M. (1987). Topographical and geological amplifications determined from the strong-motion and aftershock records of the 3 March 1985 Chile earthquake, *Bull. Seism. Soc. Am.* **77**, 1147–1167.
- Celebi, M., J. Prince, C. Dietel, M. Onate, and G. Chavez (1987). The culprit in Mexico City—amplification of motions, *Earthquake Spectra* **3**, 315–328.
- Chen, P. C. (1985). Vertical distribution of peak subsurface horizontal earthquake accelerations, Report to the National Science Foundation.
- Cockerham, R. S. and E. J. Corbett (1987). The July 1986 Chalfant Valley, California, earthquake sequence: preliminary results, *Bull. Seism. Soc. Am.* **77**, 280–289.
- Converse, A. (1984). AGRAM: a series of computer programs for processing digitized strong-motion accelerograms. Version 2.0, *U.S. Geol. Surv., Open-File Rept. 84-525*.
- Fumal, T. E., R. E. Warrick, E. C. Etheridge, and R. J. Archuleta (1985). Downhole geology, seismic velocity structure and instrumentation at the McGee Creek, California, recording site, *Earthquake Notes* **55** (1), 5.
- Hauksson, E., T.-L. Teng, and T. L. Henyey (1987). Results from a 1500 m deep, three-level downhole seismometer array: site response, low  $Q$  values, and  $f_{max}$ , *Bull. Seism. Soc. Am.* **77**, 1883–1904.
- Jarpe, S. P., C. H. Cramer, B. E. Tucker, and A. F. Shakal (1988). A comparison of observations of ground response to weak and strong motion at Coalinga, California, *Bull. Seism. Soc. Am.* **78**, 421–435.
- Joyner, W. B., R. E. Warrick, and A. A. Oliver, III (1976). Analysis of seismograms from a downhole array in sediments near San Francisco Bay, *Bull. Seism. Soc. Am.* **66**, 937–958.
- Joyner, W. B., R. E. Warrick, and T. E. Fumal (1981). The effect of quaternary alluvium on strong ground motion in the Coyote Lake, California, earthquake of 1979, *Bull. Seism. Soc. Am.* **71**, 1333–1349.
- Liu, H.-P., R. E. Warrick, R. E. Westerlund, J. B. Fletcher, and G. L. Maxwell (1988). An air-powered impulsive shear-wave source with repeatable signals, *Bull. Seism. Soc. Am.* **78**, 355–369.
- Maley, R. P., E. C. Etheridge, and A. Acosta (1986). U.S. Geological Survey strong-motion records from the Chalfant Valley, California, earthquake of July 21, 1986, *U.S. Geol. Surv., Open-File Rept. 86-568*.

- Malin, P. E., J. A. Waller, R. D. Borchardt, E. Cranswick, E. G. Jensen, and N. Van Schaack (1988). Vertical seismic profiling of Oroville microearthquakes: velocity spectra and particle motion as a function of depth, *Bull. Seism. Soc. Am.* **78**, 401–420.
- Malin, P. E., T. McEvilly, and T. Moses (1987). Cooperative UCSB-UCB-USGS recovery and instrumentation of the 5150 ft Varian A-1 well as a geophysical observatory (abstract), *EOS* **68**, 1357.
- Mitchell, D. (1987). Structural damage due to the 1985 Mexican earthquake, *Proc. Fifth Canadian Conf. Earthquake Engineering*, 6–8 July, Ottawa, Canada, 87–111.
- Mueller, C. S. (1986). The influence of site conditions on near-source high-frequency ground motion: case studies from earthquakes in Imperial Valley, Ca., Coalinga, Ca., and Miramichi, Canada, *Ph.D. Thesis*, Stanford University, Stanford, California.
- Omote, S., Y. Ohsawa, B. Ohmura, S. Iizuka, T. Ohta, and K. Takahashi (1984). Observation of earthquake strong-motion with deep boreholes—an introductory note for Iwaki and Tomioka observation station in Japan, *Proc. Eighth World Conf. Earthquake Engineering*, Vol. 2, 21–28 July, San Francisco, 247–254.
- Priestly, K. F., K. D. Smith, and R. S. Cockerham (1988). The 1984 Round Valley, California earthquake sequence, *Geophys. J. R. Astr. Soc.* **95**, 215–235.
- Redpath, B. B. and R. C. Lee (1986). In-situ measurements of shear-wave attenuation at a strong motion recording site (abstract), *Earthquake Notes* **57** (1), 8.
- Rogers, A. M., J. C. Tinsley, and R. D. Borchardt (1985). Predicting relative ground response, *Evaluating Earthquake Hazards in the Los Angeles Region—An Earth-Science Perspective*, J. I. Ziony (Editor), *U.S. Geol. Surv. Profess. Paper* 1360, 221–247.
- Sangas, P., R. J. Archuleta, and L. M. Baker (1989). Design, installation and digital recording of a downhole seismic accelerometer array at Lake Hemet, Ca., near the San Jacinto fault (abstract), *Seism. Res. Lett.* **60**, 4.
- Seale, S. H. and R. J. Archuleta (1988). Site Effects at McGee Creek, California, *Earthquake Engineering and Soil Dynamics II—Recent Advances in Ground-Motion Evaluation, Proc. of the A.S.C.E. Specialty Conference*, 27–30 June, Park City, Utah, 173–187.
- Seed, H. B. and I. M. Idriss (1970). Analysis of ground motions at Union Bay, Seattle, during earthquakes and distant nuclear blasts, *Bull. Seism. Soc. Am.* **60**, 125–136.
- Seed, H. B., M. P. Romo, J. I. Sun, A. Jaime, and J. Lysmer (1988). The Mexico earthquake of September 19, 1985—relationships between soil conditions and earthquake ground motions, *Earthquake Spectra* **4**, 687–729.
- Spudich, P. and E. Cranswick (1984). Soil strains and horizontal propagation velocities of strong ground motions observed during the 1979 Imperial Valley, California, earthquake, *Proc. Eighth World Conf. Earthquake Engineering*, Vol. 2, 21–28 July, San Francisco, 231–238.
- Tucker, B. E. and J. L. King (1984). Dependence of sediment-filled valley response on input amplitude and valley properties, *Bull. Seism. Soc. Am.* **74**, 153–165.

INSTITUTE FOR CRUSTAL STUDIES  
UNIVERSITY OF CALIFORNIA  
SANTA BARBARA, CALIFORNIA 93106  
(S.H.S.)

DEPARTMENT OF GEOLOGICAL SCIENCES AND  
INSTITUTE FOR CRUSTAL STUDIES  
UNIVERSITY OF CALIFORNIA  
SANTA BARBARA, CALIFORNIA 93106  
(R.J.A.)

Manuscript received 19 October 1988